

Electron pair emission from a highly correlated material

F. O. Schumann,^{1,*} L. Behnke,¹ C. H. Li,¹ J. Kirschner,^{1,2} Y. Pavlyukh,² and J. Berakdar²

¹Max-Planck-Institut für Mikrostrukturphysik, Weinberg 2, D-06120 Halle, Germany

²Institut für Physik, Martin-Luther-Universität Halle-Wittenberg, 06099 Halle, Germany

(Received 16 April 2012; published 20 July 2012)

Electron pair emission spectroscopy ($e,2e$) is a tool well suited to probe the electron correlations. The probability of the electron pair emission depends in a crucial way on the localization properties of the electron wave functions describing the initial state of the system. One expects an enhanced coincidence signal from the localized electron states in oxides compared to that of itinerant states in metals. Our comparative ($e,2e$) study of the Ag(001) and NiO/Ag(001) system confirms this observation. We demonstrate that the intensity of the pair emission increases by an order of magnitude after the deposition of 15 monolayers of NiO onto the Ag(001) substrate.

DOI: [10.1103/PhysRevB.86.035131](https://doi.org/10.1103/PhysRevB.86.035131)

PACS number(s): 73.20.At, 79.60.—i

I. INTRODUCTION

Effective single-particle theories turned out to be highly efficient and surprisingly successful in describing the properties of a wide range of systems. Nonetheless, electronic correlations beyond the single-particle picture have been shown to play a key role in determining the electronic, magnetic, and optical properties of an important class of the “strongly correlated materials,” such as transition-metal oxides (TMOs).

A generic model that captures some marked effects of electronic correlations is the Hubbard model that includes, in addition to the effective single-particle energy, an energy term U that corresponds to the two-particle on-site correlation.¹ The model has been used to describe a broad range of materials and also found applications in *ab initio* calculations: Employing U as a parameter in the local-density approximation (LDA) leads to the so-called LDA + U framework and improves significantly the performance of LDA when compared with experimental findings, e.g., with the spectral functions of correlated materials such as TMO. For instance, LDA predicts a metallic behavior for NiO and CoO at odds with the experimental observation.² As a matter of fact NiO and CoO are antiferromagnetic charge-transfer insulators with a band gap of the order 4 eV. These properties are correctly reproduced by the LDA + U theory.^{3,4} From this discussion we learn that NiO and CoO can be viewed as strongly correlated materials that require to go beyond the effective single electron picture for its description.

Experimentally, the electron pair emission spectroscopy emerged as a suitable tool to probe directly the electron-electron interaction in solids, e.g., as it is manifested in the so-called exchange-correlation hole^{5,6} that results from the Pauli principle and the mutual Coulomb interaction of the electrons. In this correlation spectroscopic method, which is employed in this work, an electron pair is detected in coincidence upon the impact of one electron [also called ($e,2e$), i.e., one electron in and two out] or one vacuum ultraviolet (VUV) photon. In general the experiment can be performed in the transmission or in the reflection mode and yields qualitatively different information depending on the energies and momenta of the electron pair, as well as on whether the experiment resolves for the electron’s spin projections. For example, it was demonstrated that this technique can access

the one-electron (spin-resolved) spectral function.^{7–13} For low energies the mechanisms of electron-electron collisions at surfaces can be studied.^{14–18} Further studies revealed the role of the surface dielectric response on the correlated pair emission.^{19–22} For a fast incoming electron (>100 eV) and a small energy and momentum loss (i.e., for a small momentum transfer) of this electron the pair-correlation technique delivers related spectroscopic information as done by the angle-resolved photoemission spectroscopy (ARPES)^{23,24} (using linearly polarized photons). For the pair emission technique however, electronic transitions with a large wave vector change can be induced at moderate impact energy. In addition, for ($e,2e$) the projectile effective electric field acting on the surface electrons is along the momentum transfer.²⁵ In contrast, for ARPES the electric field is perpendicular to the momentum transfer (photon momentum). Furthermore, as demonstrated experimentally and theoretically, the pair emission is particularly surface sensitive.

A relatively less studied system with pair-correlation spectroscopy are transition-metal oxides. A recent theoretical study on the double photoemission (DPE) from strongly correlated materials^{26,27} within the dynamical mean-field theory predicted an increase of the pair emission intensity with U . The connection of the electron-induced pair emission with the electron-electron interaction, as also studied in DPE, was exposed in a previous work.²⁸ The relationship between the pair emission probability induced by VUV photons and U can be heuristically understood as follows. Due to the single-particle nature of the electron-photon coupling, the photon interacts with only one electron at a time. A coherent emission of a second electron depends crucially on the strength of the electron-electron interaction which is strongest when the two electrons are on the same site.^{26,27} Approaching the metallic regime (i.e., for a small U measured in units of the bandwidth) the pair occupation decreases and the coherent pair emission is expected to be lower. In fact, it was shown by formal analysis that generally the photoinduced pair emission is only possible for correlated initial or final states.²⁹ Experimentally, finite DPE intensities from Cu surfaces were observed^{8,30,31} in which case the electron pairs are expected to be emitted from a region with an extent set by the screening length. From this picture we expect that the correlated pair emission

spectroscopy carries information on the short-range electronic correlation.

In this work we present experimental ($e,2e$) spectra for two typical TMOs, NiO and CoO, and contrast them with measurements for noble metals with a special attention to the U dependence of the pair emission probability. Comparing the coincidence spectra from Ag and NiO provides the opportunity to test the conjecture of a U dependence. A convenient fact is that the preparation of NiO films on a Ag(100) substrate is well documented.^{32–38} This simplifies the comparison of these two materials under otherwise identical experimental conditions. We prepared NiO films on a Ag(100) substrate and investigated the electron pair intensity over a primary energy range of 25–75 eV. Experimentally we observe that the pair emission intensity of NiO is an order of magnitude larger than for Ag. We also present first results on other metal oxides which demonstrate that an enhanced coincidence rate from the oxide phase compared to the metal phase is the rule rather than the exception.

The experiment is supported by LDA + U calculations for NiO/Ag(100). In addition to the structural and the magnetic characterization of the oxide films we show that the enhanced pair emission indeed stems from the electronic states of NiO oxide and is not related to the substrate or to the hybridized electronic states responsible for the chemical bonding. To rule out the latter the layer projected electronic structure was computed using the projected augmented wave (PAW) formalism,³⁹ as implemented in the ABINIT 6.0 program package.^{40,41} Our calculations show that the bonding between the oxide and the metallic substrate is relatively weak resulting in increased O-Ag distances in line with x-ray-absorption spectroscopy.⁴²

II. METHODS

A. Experiment

A sketch of the overall layout of the experiment is shown in Fig. 1 which has been described in more detail elsewhere.^{43–45} It consists of two hemispherical electron energy analyzers with a mean radius of 200-mm equipped wide angle transfer lenses and position sensitive detectors.⁴⁶ We use channel plate detectors with resistive anodes.⁴⁷ All experiments are performed with the primary beam parallel to the surface normal. The overall energy resolution of the setup is ≈ 0.7 eV as judged from the sum energy spectra to be shown below. The contribution of the electron gun was 0.3 eV due the use of a BaO cathode.⁴⁸ The effect of the earth magnetic field has been reduced by using external Helmholtz coils and a μ -metal chamber. The base pressure of the chamber was $\approx 4 \times 10^{-11}$ mbar.

The Ag(100) surface was cleaned via established procedures. Following the bakeout the surface was initially sputtered with 1-keV Ar⁺ ions for 24 h. This was followed by cycles of 15 min sputtering and subsequent annealing to 750 K; this resulted in a sharp low-energy electron diffraction (LEED) pattern indicating a well-ordered surface. The NiO films were prepared via Ni evaporation in a O₂ atmosphere of 10^{-6} mbar. The Ag crystal was held at a temperature of 470 K while the growth rate was approximately 0.5 monolayer (ML)/min. These parameters are well documented in the literature to result

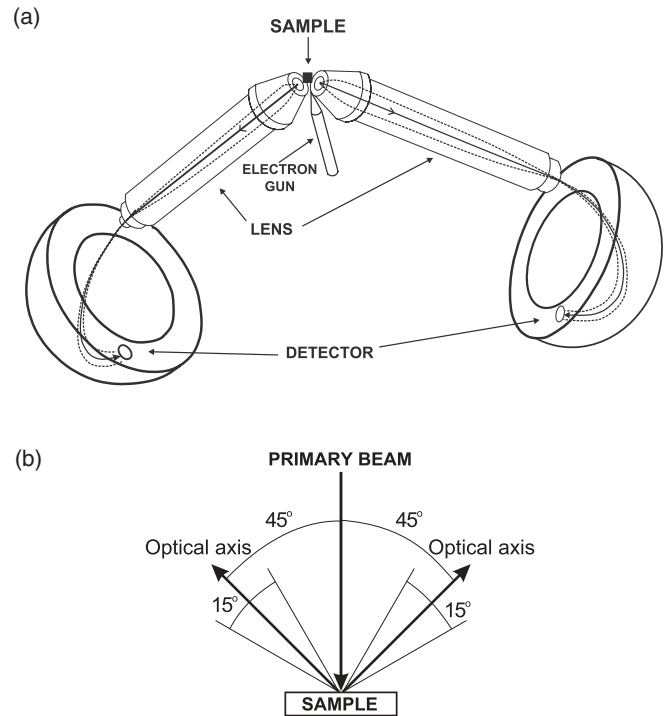


FIG. 1. (a) Sketch of the coincidence electron spectrometer. It shows two hemispherical electron energy analyzers that define a scattering plane. The [011] direction of the Ag(100) surface lies within the scattering plane. (b) The transfer lenses of the spectrometers are symmetrically positioned in the same plane as the primary beam. The outgoing electrons are detected at $\pm 45^\circ$ with respect to the surface normal. The angular acceptance range of $\pm 15^\circ$ with respect to mean take-off angle is also shown.

in a well-ordered NiO film which is confirmed by our LEED observations. The azimuthal orientation of the sample was such that the [011] direction was in the scattering plane defined by the electron-optical axis of the spectrometer. During the ($e,2e$) experiments the sample was kept at room temperature. The primary energy and the kinetic energy of the outgoing electrons are quoted with respect to the vacuum level of the sample. Due to the integration over all emission angles within the angular acceptance we probe valence states centered within 0.4 \AA^{-1} of the Γ point.⁴⁵ We employ a four-way coincidence circuit in which the channel plate signals originating from the two spectrometers have to be within a time interval of 100 ns while at the same time the electronics of the resistive anodes indicate a successful impact position determination. The latter is required to determine the kinetic energy E_{left} and E_{right} of the coincident electrons. If a valid event is registered the arrival times (t_{left} and t_{right}) with respect to the coincidence trigger can be determined. With this it is straightforward to determine the arrival time difference $dt = t_{\text{left}} - t_{\text{right}}$ for a coincidence event which leads to a dt histogram (Fig. 3).

B. Theory

In order to model a NiO/Ag(100) layered system we performed two slab calculations (plane-wave basis, kinetic-energy cutoff of 50 a.u., projected augmented wave (PAW) method with 3 and 5 monolayers of NiO on top of 5 and

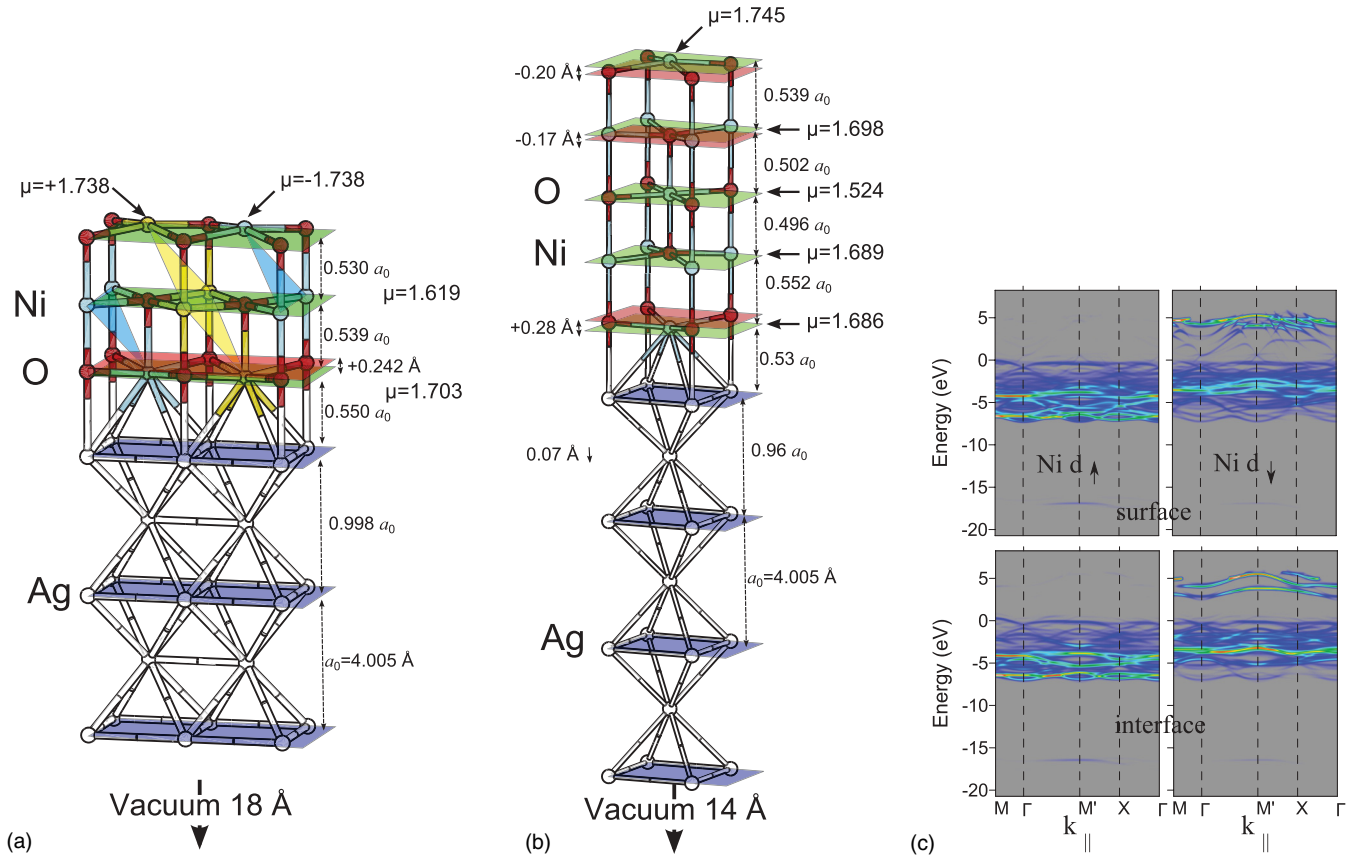


FIG. 2. (Color) Results of the structural optimization and magnetic properties for the AF₂ magnetic configuration of (a) 3 MLs and (b) 5 MLs of NiO at Ag(100). The NiO-Ag interlayer distance differs slightly for 3 and 5 monolayers (3 MLs, 5 MLs): 2.20 and 2.12 Å, respectively. Calculations predict the O-on-top configuration and a slight bulking of the surface (−0.20 Å) and interface (+0.28 Å) Ni atoms. Panel (c) displays the spin-resolved AF₂ band structure projected onto the *d* states of surface and interface Ni atoms.

7 Ag metal layers, respectively (Fig. 2). For the LDA + *U* calculations we use values of the Hubbard parameters $U = 8$ eV and $J = 0.95$ eV as suggested by Anisimov, Zaanen, and Andersen.² This is not a unique choice. A number of recent works address the problem of *ab initio* determination of these parameters. A detailed discussion of relevant physical properties of transition-metal oxides as a function of these parameters can be found in a recent work.⁴

Integration of the Brillouin zone is typically done using the $6 \times 6 \times 4$ Monkhorst-Pack grid. Geometry relaxation of Ni and O was performed for nonmagnetic configurations, while the Ag atoms were fixed at the crystallographic positions corresponding to the optimized lattice constant of 4.005 Å. Thus the theoretical Ag lattice is underestimated by 2% compared to the experiment. This is a typical trend for the local-density approximation. The structural optimization for nonmagnetic phase is followed by the band-structure calculations for the converged geometry and AF₂ antiferromagnetic configuration. The resulting geometry is in good agreement with experimental extended x-ray-absorption fine-structure (EXAFS) data and theoretical calculations.^{42,49}

III. RESULTS

A key motivation of this work is to compare the coincidence intensity from a metal, e.g., Ag and from NiO in order to

address a dependence on the model parameter *U*. A convenient way is to look at the arrival time difference *dt* spectrum for Ag and NiO for all coincidences within a certain energy window (Fig. 3). Both spectra have been obtained under essentially the same conditions for the data acquisition time of 24 h. The acceleration voltage of the primary electron was fixed, as was the primary flux. The analyzers were set to probe the same energy window. It is obvious that both distributions display a peak centered at $dt \approx 0$ ns; the small shift towards smaller *dt* values is due to a small time offset in the signal chains. The width of the peaks is in both instances approximately 10 ns, which reflects the time resolution of the experiment. The emergence of a peak is clear proof of *true* coincidences. These events stem from the impact of one primary electron. Within the time resolution of the experiment these correlated electrons leave the sample at the same time and hence will be detected at the same time. The intensity outside the peak region is due to *random* coincidences. These events are caused by the impact of two primary electrons within the time window of the coincidence circuit (100 ns in our case). Therefore the *dt* spectrum gives us immediately the ratio of *true* to *random* coincidences. The key observation is a significantly higher intensity peak for NiO compared to Ag (a factor of 8 in this example). The ratio of *true* to *random* coincidences is 8.5 for NiO compared to 4.7 for Ag.

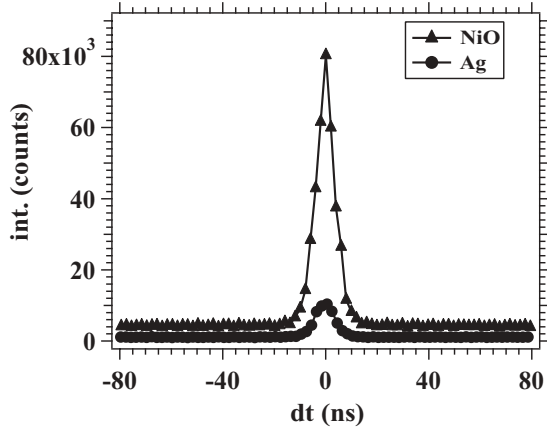


FIG. 3. Arrival time difference spectrum obtained from a Ag(100) surface and a 15-ML NiO/Ag(100) film. The acceleration voltage of the primary beam was kept constant at 32 V. Due to variations of the work function and positions of the chemical potential the primary energy is $E_p = 30$ eV for Ag(100) and $E_p = 31.6$ eV for NiO/Ag(100). The data acquisition for both experiments was 19 h and the primary flux was constant. The peak in the spectrum is the signature of *true* coincidences. The width of the peak reflects the time resolution of the instrument. Corresponding energy spectra are compared in Figs. 4 and 5.

We conclude that the pair emission from a material described with a $U = 8$ eV is significantly increased compared to a material with $U \approx 0$. This supports the view that the statements made about the DPE intensity versus U can be at least qualitatively extended to a $(e, 2e)$ process.

For further ease of presentation it is useful to recall the energy conservation within a $(e, 2e)$ process. For simplicity we discuss the case of a metal; the extension to an insulator is straightforward. The energy before and after the scattering event has to be preserved, hence

$$E_p + E_{VB} = E_{\text{left}} + E_{\text{right}} + \phi = E_{\text{sum}} + \phi. \quad (1)$$

In this formula the primary electron energy is given by E_p while the binding energy of the valence electron is determined by E_{VB} . The usual convention is to set $E_{VB} = 0$ for states at the Fermi level E_F . The kinetic energies of the emitted electrons are E_{left} and E_{right} , respectively. Since we effectively remove one electron from the sample we have to take into account the work function ϕ of the sample. The work function of a Ag(100) surface is 4.6 eV. The outgoing electron pair is characterized by the sum energy $E_{\text{sum}} = E_{\text{left}} + E_{\text{right}}$. We rearrange Eq. (1) and obtain

$$E_{\text{sum}} = E_p + E_{VB} - \phi. \quad (2)$$

The maximum value E_{sum} can attain is labeled $E_{\text{sum}}^{\text{max}}$ and it holds $E_{\text{sum}}^{\text{max}} = E_p - \phi$. Lines of constant sum energy appear in a two-dimensional (2D)-energy distribution as diagonal lines. In Fig. 4(a) we show the 2D-energy spectrum and the resulting E_{sum} spectrum from the Ag(100) surface excited with $E_p = 30$ eV. The black diagonal line marks the position of $E_{\text{sum}}^{\text{max}}$. Events at this energy location are due to emission from the highest occupied state which in a metal is the Fermi level E_F . Clearly, the emission starts once the energy coordinate falls below this line. We can easily identify two diagonal intensity

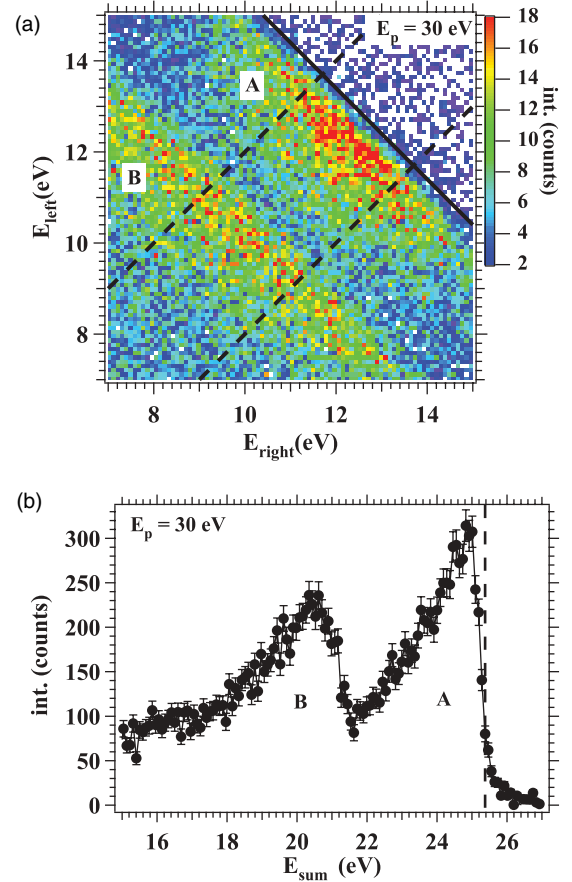


FIG. 4. (Color) Energy spectra from a Ag(100) surface excited with $E_p = 30$ eV. Panel (a) shows the 2D-energy spectrum, where the solid diagonal line marks the position of $E_{\text{sum}}^{\text{max}}$. Two bands of high intensity are marked with A and B, respectively. The two dashed diagonal lines indicate the constraint $|E_{\text{left}} - E_{\text{right}}| \leq 2$ eV, which has been used to compute the E_{sum} spectrum plotted in panel (b). $E_{\text{sum}}^{\text{max}}$ is indicated by a vertical dashed line. The contributions from the intensity bands labeled A and B in (a) result in peaks in the E_{sum} spectrum, which we label accordingly.

bands within the 2D-energy spectrum, which we label with A and B, respectively. Diagonals which are parallel to the $E_{\text{sum}}^{\text{max}}$ line identify events which originate from states with a constant binding energy. With this in mind it is natural to plot the coincidence intensity as a function of E_{sum} . We focus on almost equal energies by the constraint $|E_{\text{left}} - E_{\text{right}}| \leq 2$ eV. This energy selection is identified by the dashed diagonal lines in Fig. 4(a). The resulting E_{sum} spectrum is plotted in Fig. 4(b) where the position of $E_{\text{sum}}^{\text{max}}$ is marked by the dashed vertical line. The onset of pair emission occurs right at this energy and the sharpness of the intensity variation is a measure of the energy resolution of our experiment. We quote a value of 0.7 eV. The diagonal intensity bands visible in Fig. 4(a) show up as peaks in the E_{sum} spectrum. Region A has its peak close to the Fermi level whereas region B has the maximum intensity 5 eV below E_F .

In simple terms the valence-band structure of Ag can be described by rather flat $4d$ bands and a strongly dispersing sp band. Energetically the $4d$ bands are localized in a window 3–7 eV below E_F . The sp band covers a region from 7 eV

below E_F up to the E_F . The flat $4d$ bands lead to a region of high density of states (DOS) compared to a low contribution due to the sp states. With this in mind we can identify region B to emanate from the $4d$ states whereas the intensity of region A stems from the sp states. We should emphasize that the $(e,2e)$ intensity spectrum is not a simple replica of the DOS. However, a finite $(e,2e)$ intensity requires nonvanishing occupation of valence states within the energy and momentum window of the experiment. With this in mind we can easily understand the strong intensity of region B. The high intensity and the peak in region A is somewhat surprising, because the DOS is rather low and does not display a peak. This is clear evidence that for a full interpretation of the spectra complete $(e,2e)$ calculations are required. In Fig. 5 we display the energy spectra from a 15-ML NiO/Ag(100) film together with a calculated binding energy spectrum on the basis of the band structure displayed in Fig. 2(c). In panel (a) we show the 2D-energy spectrum and see that the onset of pair emission occurs near the black diagonal lines which indicates the position of $E_{\text{sum}}^{\text{max}}$. Slightly below this line we see a diagonal line which suggests the relevance of valence states of particular binding energies. However, most of the intensity is centered at around the position (12 eV, 12 eV) and no prominent diagonal lines like in the Ag(100) case [see Fig. 4(a)] can be seen. From the 2D-energy spectrum we can compute the E_{sum} spectrum. Due to the better statistics a more stringent constraint $|E_{\text{left}} - E_{\text{right}}| \leq 1$ eV can be selected as indicated by the dashed diagonal lines. The band structure of NiO is in simple terms described by rather flat $3d$ bands which result in well-defined regions of high density of states. The width of the valence band in the LDA + U approach is 7 eV [Fig. 2(c)].

We can use the band-structure calculation and compute the DOS as a function of the binding energy and compare this with the E_{sum} spectrum. The geometry of the experiment and the almost equal energy of the emitted electrons set the kinematically accessible part of a region in the Brillouin zone around the Γ point within $\pm 0.4 \text{ \AA}^{-1}$. Furthermore, we employ a Gaussian broadening of 0.5 eV to account for the energy resolution. Note that, however, because of the weak dispersion, the influence of the kinematically restricted region for the k -point sampling in the Brillouin zone is not very strong. Upon the sampling we observe (Fig. 5) that the binding energy spectrum still displays well separated peaks despite the broadening. This is in contrast to the E_{sum} spectrum plotted in Fig. 5(b) where only two broad features (labeled A and B) are visible. The sum-energy spectrum is significantly wider indicating that the electron emission also originates from the satellite states as was found in the photoemission experiments.⁵⁰ We note here, also, that pair emission events accompanied with inelastic multiple scattering becomes possible as soon as the pair emission takes place from states below the top of the valence band and is expected to enhance for emission from deeper levels of the valence bands because of the increased phase space. These events are not described by band-structure calculations and require separate analysis. For example, the treatment of the satellite states requires a systematic inclusion of dynamic correlations. A first explanation for the band structure of NiO was given by Fujimori *et al.*⁵¹ on the basis of the configuration interaction approach applied to the Ni-ligand cluster. A year later Zaanen, Sawatzky, and Allen⁵² introduced their classification of TMOs

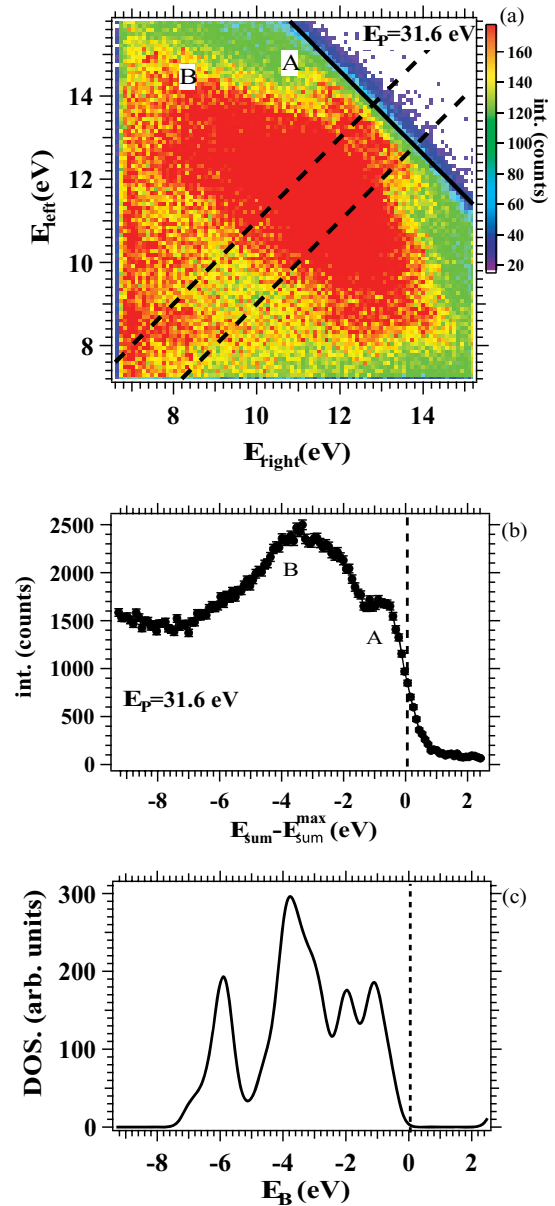


FIG. 5. (Color) Energy spectra from a 15-ML NiO/Ag(100) film excited with $E_p = 31.6$ eV. Panel (a) shows the 2D-energy spectrum, where the solid diagonal line marks the position of $E_{\text{sum}}^{\text{max}}$. The two dashed diagonal lines indicate the constraint $|E_{\text{left}} - E_{\text{right}}| \leq 1$ eV, which has been used to compute the E_{sum} spectrum in panel (b). The energy $E_{\text{sum}}^{\text{max}}$ is indicated by a vertical dashed line. For comparison we have included in panel (c) the calculated DOS spectrum obtained after integration over the kinematically accessible part of the Brillouin zone. Further, we convoluted this with a Gaussian of 0.5 eV width to take into account the experimental energy resolution.

and related compounds into Mott-Hubbard and charge-transfer CT systems and showed that NiO belongs to the second type with U larger, but comparable to the metal-ligand charge-transfer energy Δ . Besides model approaches the LDA + DMFT theory provides a method to describe the system on the *ab initio* level.⁵³

An important issue is the question whether the enhanced coincidence intensity from NiO is a genuine effect and not a consequence of the finite angular acceptance of the instrument.

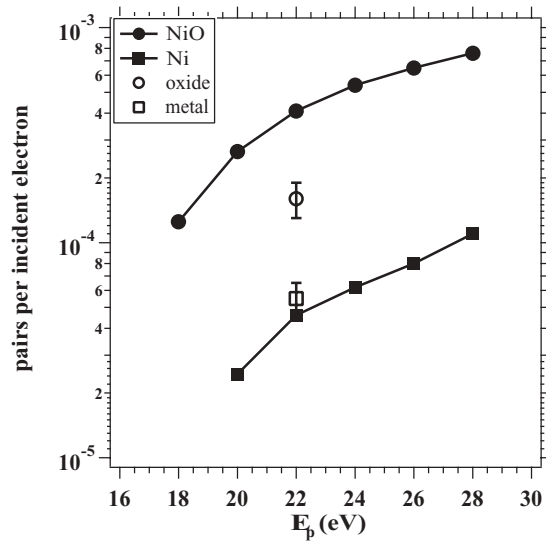


FIG. 6. Coincidence intensity measured as electron pair per incoming primary electron. Full circles and squares are the result for NiO and Ni, respectively. The result for Fe, Cr and V oxides and metal phase have been grouped together and are labeled with the open circles and squares. They indicate the average value while the error bars refer to the variance.

It is in principle conceivable that the integrated coincidence intensity from Ag(100) and NiO(100) shows no significant variation, but that the angular distributions are different such that most of the pairs from the Ag(100) surface are not within the field of view of the apparatus. In order to rule out this aspect we employed a time-of-flight spectrometer similar to the one described elsewhere.^{30,31,54} It has an angular acceptance within the scattering plane of ± 1.57 rad and perpendicular to it ± 0.40 rad. Additionally this instrument is equipped with a channel plate detector to measure the low primary flux (of the order 10^{-15} A) in absolute units. We studied besides NiO also oxides containing Fe, Cr, and V and compared the intensity from the pure metal phase. The structural order and exact chemical state requires further studies, but there is already a clear picture emerging; see Fig. 6. Making use of the possibility to measure the primary flux we quote the coincidence intensity as electron pair per incoming primary electron. We consider

all pairs within the angular acceptance and integrate over all energies.

Let us discuss the result for NiO and Ni first. For E_p values in the range 18–28 eV the pair emission for NiO is an order of magnitude more intense than for Ni. This agrees with the findings displayed in Fig. 3 where the pair emission from NiO and Ag(100) is compared. We emphasize that postoxidizing the Ni metal film does not increase the pair emission significantly. The next question is whether an increased coincidence rate is also observable for other oxides. First studies on Fe, V, and Cr metal films and their oxides performed at one primary energy are included in Fig. 6 via open circles and squares, respectively. The position of the open circle is the average of the Fe, Cr, and V oxide films, the error bar indicates the variation for the different materials. In the same manner we have grouped the metal films together, which are represented by the open squares.

IV. SUMMARY

We compared the electron pair emission from two very different electronic systems, namely Ag being a noble metal and NiO as an insulator. We find that pair emission from a NiO film is an order of magnitude stronger than from the Ag(100) substrate. A comparison of NiO and Ni films shows a similar behavior. We provide also first results on Fe, Cr, and V oxides and their metal phases. These data show a general trend that pair emission from strongly correlated materials is enhanced compared to the metals in line with the theoretical expectations.

These results need to be further substantiated by considering a theoretical model capable of describing a large class of materials from the unifying point of view. The p - d Anderson model seems to be sufficiently broad covering a range of materials from the Mott-Hubbard through the charge-transfer insulators to metallic systems as analyzed in detail by Bocquet *et al.*⁵⁵ Further comparison of experimental ($e, 2e$) intensities for these systems and development of the corresponding theory is required.

ACKNOWLEDGMENT

Funding from the DFG through SFB 762 is gratefully acknowledged.

*schumann@mpi-halle.de

¹J. Hubbard, *Proc. R. Soc. London A* **276**, 238 (1963).

²V. I. Anisimov, J. Zaanen, and O. K. Andersen, *Phys. Rev. B* **44**, 943 (1991).

³T. Cai, H. Han, Y. Yu, T. Gao, J. Du, and L. Hao, *Physica B: Condens. Matter* **404**, 89 (2009).

⁴H. Jiang, R. I. Gomez-Abal, P. Rinke, and M. Scheffler, *Phys. Rev. B* **82**, 045108 (2010).

⁵E. Wigner and F. Seitz, *Phys. Rev.* **43**, 804 (1933).

⁶J. C. Slater, *Rev. Mod. Phys.* **6**, 209 (1934).

⁷J. Kirschner, O. M. Artamonov, and S. N. Samarin, *Phys. Rev. Lett.* **75**, 2424 (1995).

⁸R. Herrmann, S. Samarin, H. Schwabe, and J. Kirschner, *Phys. Rev. Lett.* **81**, 2148 (1998).

⁹E. Weigold and I. E. McCarthy, *Electron Momentum Spectroscopy* (Kluwer Academic/Plenum, New York, 1999).

¹⁰J. Berakdar, *Phys. Rev. Lett.* **83**, 5150 (1999).

¹¹S. N. Samarin, J. Berakdar, O. M. Artamonov, and J. Kirschner, *Phys. Rev. Lett.* **85**, 1746 (2000).

¹²A. Morozov, J. Berakdar, S. N. Samarin, F. U. Hillebrecht, and J. Kirschner, *Phys. Rev. B* **65**, 104425 (2002).

¹³F. Giebels, H. Gollisch, R. Feder, F. O. Schumann, C. Winkler, and J. Kirschner, *Phys. Rev. B* **84**, 165421 (2011).

¹⁴J. Berakdar and M. P. Das, *Phys. Rev. A* **56**, 1403 (1997).

- ¹⁵J. Berakdar, S. N. Samarin, R. Herrmann, and J. Kirschner, *Phys. Rev. Lett.* **81**, 3535 (1998).
- ¹⁶H. Gollisch, T. Scheunemann, and R. Feder, *Solid State Commun.* **117**, 691 (2001).
- ¹⁷J. Berakdar, H. Gollisch, and R. Feder, *Solid State Commun.* **112**, 587 (1999).
- ¹⁸S. Samarin, O. M. Artamonov, A. D. Sergeant, R. Stamps, and J. F. Williams, *Phys. Rev. Lett.* **97**, 096402 (2006).
- ¹⁹W. S. M. Werner, A. Ruocco, F. Offi, S. Iacobucci, W. Smekal, H. Winter, and G. Stefani, *Phys. Rev. B* **78**, 233403 (2008).
- ²⁰W. S. M. Werner, F. Salvat-Pujol, W. Smekal, R. Khalid, F. Aumayr, H. Störi, A. Ruocco, and G. Stefani, *Appl. Phys. Lett.* **99**, 184102 (2011).
- ²¹K. A. Kouzakov and J. Berakdar, *Phys. Rev. Lett.* **91**, 257007 (2003).
- ²²K. A. Kouzakov and J. Berakdar, *Phys. Rev. A* **85**, 022901 (2012).
- ²³*Angle-Resolved Photoemission: Theory and Applications*, edited by S. D. Kevan (Elsevier, Amsterdam, 1992).
- ²⁴S. Hüfner, *Photoelectron Spectroscopy* (Springer, Berlin, 2003).
- ²⁵U. Fano, *Annu. Rev. Nucl. Sci.* **13**, 1 (1963).
- ²⁶B. D. Napitu and J. Berakdar, *Phys. Rev. B* **81**, 195108 (2010).
- ²⁷B. D. Napitu and J. Berakdar, *Eur. Phys. J. B* **85**, 50 (2012).
- ²⁸F. O. Schumann, J. Kirschner, and J. Berakdar, *Phys. Rev. Lett.* **95**, 117601 (2005).
- ²⁹J. Berakdar, *Phys. Rev. B* **58**, 9808 (1998).
- ³⁰F. O. Schumann, C. Winkler, and J. Kirschner, *Phys. Rev. Lett.* **98**, 257604 (2007).
- ³¹F. O. Schumann, N. Fominykh, C. Winkler, J. Kirschner, and J. Berakdar, *Phys. Rev. B* **77**, 235434 (2008).
- ³²S. Peacor and T. Hibma, *Surf. Sci.* **301**, 11 (1994).
- ³³J. Wollschläger, D. Erdös, H. Goldbach, R. Höpken, and K. M. Schröder, *Thin Solid Films* **400**, 1 (2001).
- ³⁴S. Großer, C. Hagendorf, H. Neddermeyer, and W. Widdra, *Surf. Interface Anal.* **40**, 1741 (2008).
- ³⁵M. Caffio, B. Cortigiani, G. Rovida, A. Atrei, C. Giovanardi, A. di Bona, and S. Valeri, *Surf. Sci.* **531**, 368 (2003).
- ³⁶K. Marre and H. Neddermeyer, *Surf. Sci.* **287–288**, 995 (1993).
- ³⁷K. Marre, H. Neddermeyer, A. Chassé, and P. Rennert, *Surf. Sci.* **357–358**, 233 (1996).
- ³⁸A. Dhaka, D. Sander, H. L. Meyerheim, K. Mohseni, E. Soyka, J. Kirschner, W. A. Adeagbo, G. Fischer, A. Ernst, and W. Hergert, *Phys. Rev. B* **84**, 195441 (2011).
- ³⁹F. Bottin, S. Leroux, A. Knyazev, and G. Zérah, *Comput. Mater. Sci.* **42**, 329 (2008).
- ⁴⁰X. Gonze *et al.*, *Z. Kristallogr.* **220**, 558 (2005).
- ⁴¹X. Gonze *et al.*, *Comput. Phys. Commun.* **180**, 2582 (2009).
- ⁴²C. Lamberti, E. Groppo, C. Prestipino, S. Casassa, A. M. Ferrari, C. Pisani, C. Giovanardi, P. Luches, S. Valeri, and F. Boscherini, *Phys. Rev. Lett.* **91**, 046101 (2003).
- ⁴³G. A. van Riessen, F. O. Schumann, M. Birke, C. Winkler, and J. Kirschner, *J. Phys.: Condens. Matter* **20**, 442001 (2008).
- ⁴⁴G. van Riessen, Z. Wei, R. S. Dhaka, C. Winkler, F. O. Schumann, and J. Kirschner, *J. Phys.: Condens. Matter* **22**, 092201 (2010).
- ⁴⁵F. O. Schumann, R. S. Dhaka, G. A. van Riessen, Z. Wei, and J. Kirschner, *Phys. Rev. B* **84**, 125106 (2011).
- ⁴⁶N. Mårtensson, P. Baltzer, A. Brambilla, P. A. Brühwiler, J. O. Forsell, A. Nilsson, A. Stenborg, and B. Wannberg, *J. Electron. Spectrosc. Relat. Phenom.* **70**, 117 (1994).
- ⁴⁷Quantar Technology Incorporated, Model 3300 SERIES MCP.
- ⁴⁸Kimball Physics, Model ELG-2.
- ⁴⁹F. Cinquini, L. Giordano, G. Pacchioni, A. M. Ferrari, C. Pisani, and C. Roetti, *Phys. Rev. B* **74**, 165403 (2006).
- ⁵⁰G. A. Sawatzky and J. W. Allen, *Phys. Rev. Lett.* **53**, 2339 (1984).
- ⁵¹A. Fujimori, F. Minami, and S. Sugano, *Phys. Rev. B* **29**, 5225 (1984).
- ⁵²J. Zaanen, G. A. Sawatzky, and J. W. Allen, *Phys. Rev. Lett.* **55**, 418 (1985).
- ⁵³J. Kuneš, V. I. Anisimov, A. V. Lukoyanov, and D. Vollhardt, *Phys. Rev. B* **75**, 165115 (2007).
- ⁵⁴F. O. Schumann, C. Winkler, and J. Kirschner, *New J. Phys.* **9**, 372 (2007).
- ⁵⁵A. E. Bocquet, T. Mizokawa, T. Saitoh, H. Namatame, and A. Fujimori, *Phys. Rev. B* **46**, 3771 (1992).